INTERNATIONAL ATOMIC ENERGY AGENCY
UNITED NATIONS EDUCATIONAL, SCIENTIFIC AND CULTURAL ORGANIZATION

INTERNATIONAL CENTRE FOR THEORETICAL PHYSICS
34100 TRIESTE (ITALY) - P.O.B. 586 - MIRAMARE - STRADA COSTIERA 11 - TELEPHONE: 2240-1
CABLE: CENTRATOM - TELEX 460392-I

H4.SMR/222 - 24

SECOND AUTUMN WORKSHOP ON

CLOUD PHYSICS AND CLIMATE

(23 November - 18 December 1987)

CLOUD & PRECIPITATION PROCESSES

Part II. NON-PRECIPITATING CLOUD SYSTEMS

G. Vali

University of Wyoming
U.S.A.

STRATUS, STRATOCUMULUS –

– CLOUD TOPPED BOUNDARY LAYER

NEIBURGER et al 1961

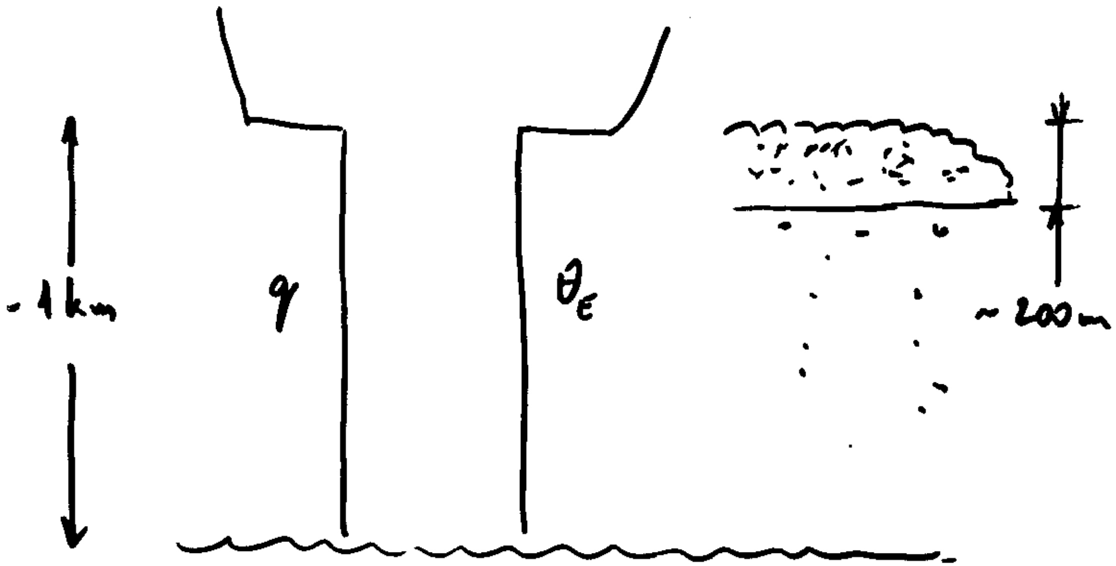

PERCENT OF OBS. WITH INVERSIONS
JUNE – SEPT.

- SUBSIDENCE ALOFT; EAST OF HIGHS
- DIURNAL CYCLE
- VARIATION OF INVERSION HT. NEAR COAST

- GLOBAL IMPACT

FIGURE 3. VERTICAL CROSS-SECTION DEPICTING TEMPERATURE DISTRIBUTION AND LOCATION OF STRATUS CLOUD UPWIND OF THE VANDENBERG COASTLINE AT APPROXIMATELY 2000 LDT ON 13 JULY 1973.

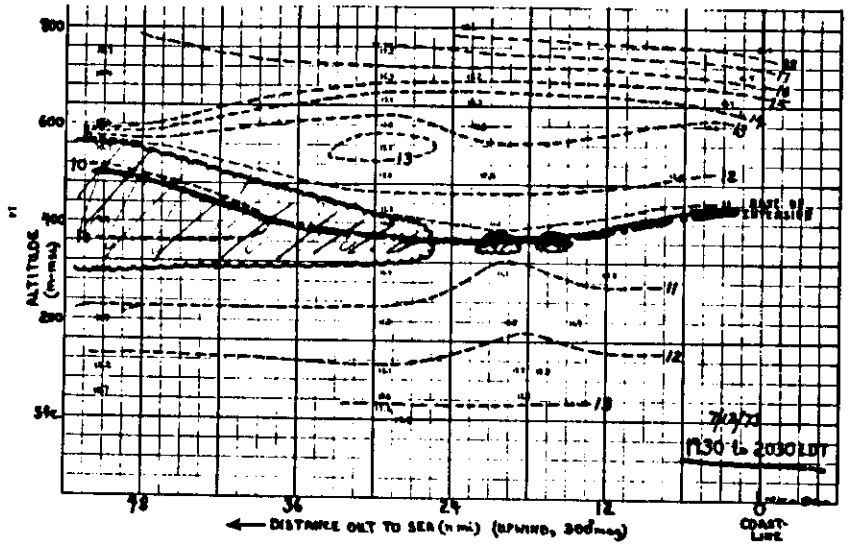

FIGURE 4. VERTICAL CROSS-SECTION DEPICTING TEMPERATURE DISTRIBUTION AND LOCATION OF STRATUS CLOUD UPWIND OF THE VANDENBERG COASTLINE AT APPROXIMATELY 0530 LDT ON 14 JULY 1973.

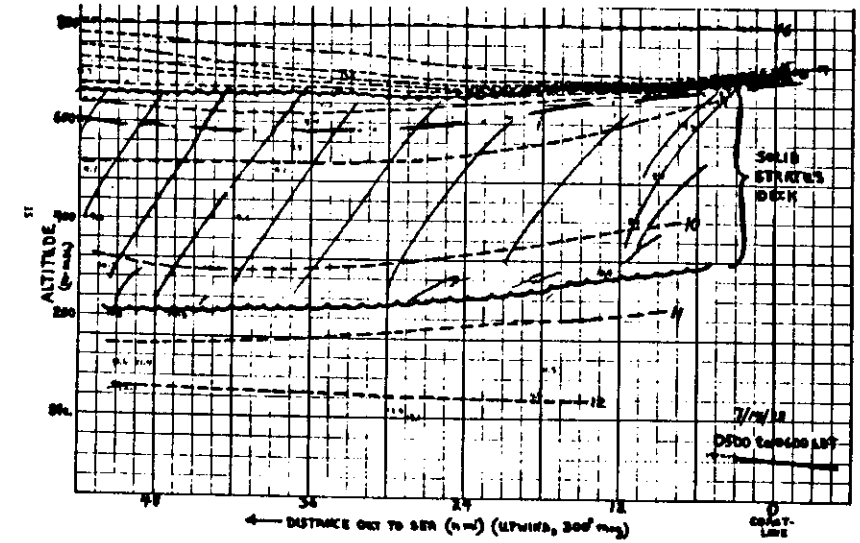

TEMPERATURE CHANGES DURING FORMATION AND DISSIPATION OF WEST COAST STRATUS *

By Morris Neiburger

The University of California at Los Angeles

(Manuscript Received, June 6, 1944)

ABSTRACT

At three-hourly intervals during three 24- to 48-hour periods in the summer of 1943, radiosonde observations were made at the University of California at Los Angeles, to ascertain the changes in vertical temperature distribution during typical stratus situations. These observations show that the base of the subsidence inversion characteristic of all summer soundings in this region undergoes marked diurnal variations in height and temperature. Computations show that advection can account for only part of the cooling at the inversion base during the formation of stratus over the station, while radiational exchange tends to raise the temperature there, rather than to lower it. Turbulence is shown to be practically negligible, and convection to play only a slight role. *Vertical motion* is found to account for the otherwise unexplained changes in temperature and inversion height. A possible cause of vertical motion with diurnal period is convergence in the land and sea breeze.

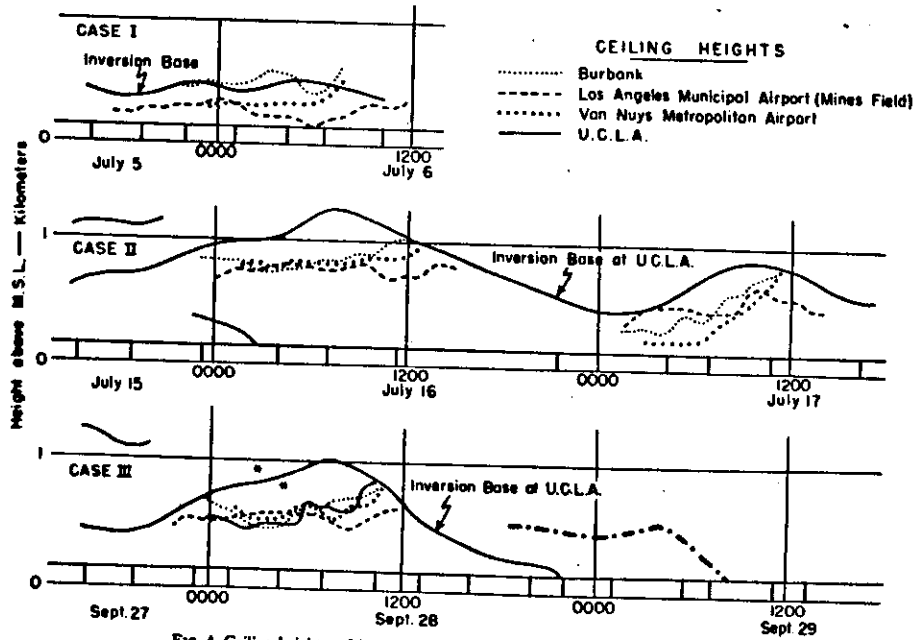

FIG. 4. Ceiling height and inversion height during U.C.L.A. Stratus Series, 1943.

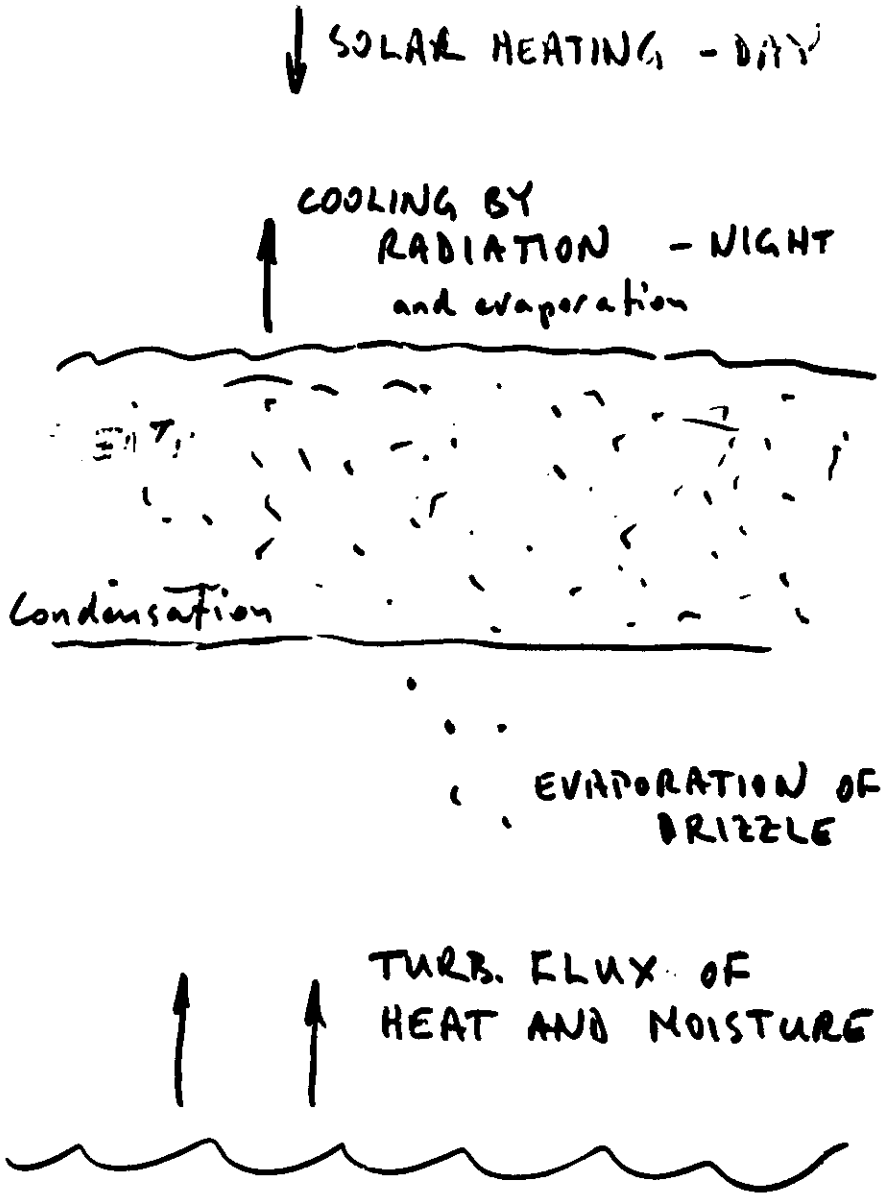

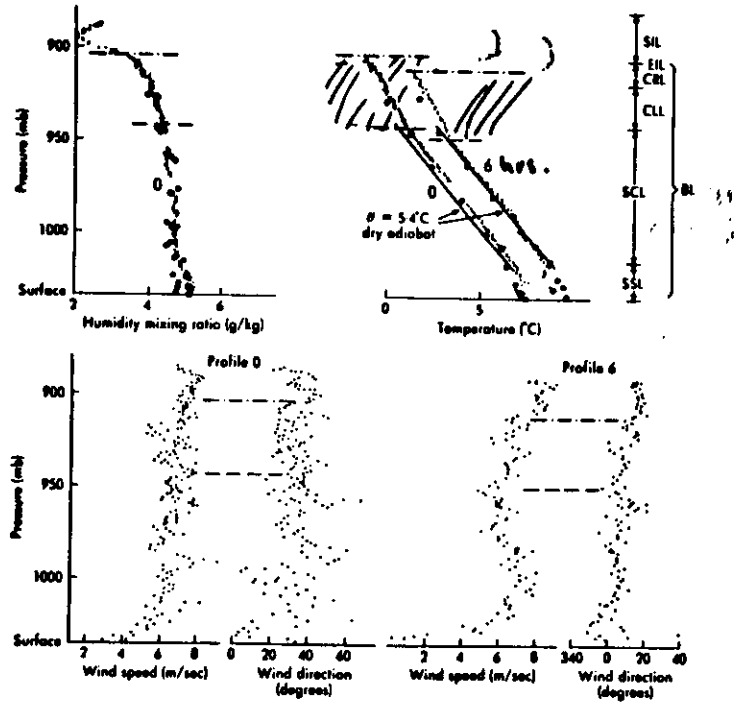

Figure 4. (a) Observations of temperature and humidity (b) Observations of wind speed and direction.
The temperature and humidity profiles are labelled with profile number from Fig. 3.
Tethered balloon observations ·
BALTHUM observations at 2300/19 ●
BALTHUM observations at 0500/20 ○
Location of cloud top — · — · —
Location of cloud base — — — —
The temperature scale refers to Profile 0; Profile 6 is displaced 2 °C to the right of Profile 0.
The layer acronyms are defined in the text.

(d) Vertical Profiles

temperature some 2°C higher.

Winds in the cloud layer observed from the tethered balloon (Fig. 4) were combined with 900m wind observations from radio-sonde stations made at 1800 0000 and 0600 in an attempt to construct the wind field within the cloud layer. Wind-field vectors (which were markedly ageostrophic) were used to estimate the trajectories of cloudy air downstream from Cardington. Points on Fig. 2 show the positions of air parcels at the chart times 'released' from Cardington (C) at 2100, 0000 and 0300 respectively. The 2100 and 0000 parcels reach the clear band some four and one and a half hours respectively after leaving Cardington, while the 0300 parcel is approaching the cloud edge three hours after release. This analysis also showed the cloud was generally dispersing along the northern edge and forming along the southern edge of the cloudless band.

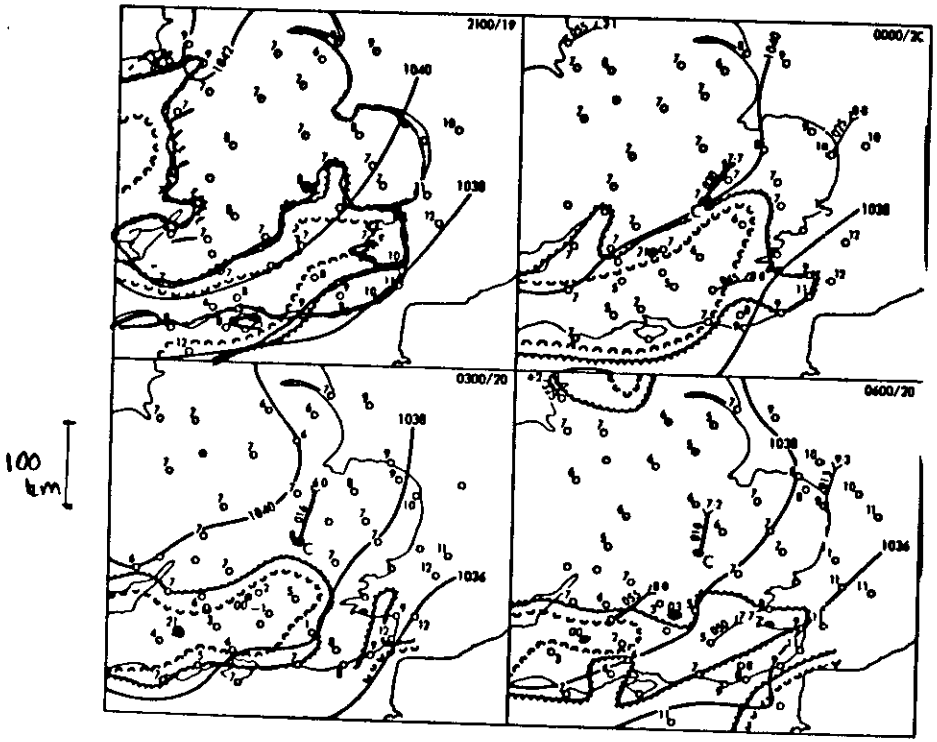

Figure 2. Observations of screen temperature at 2100, 0000, 0300, 0600 on the night of 19/20 November 1976.

Cardington (c)
Isobars (mb) ———
4 okta isoneph
7 okta isoneph
900 m wind speed (ms^{-1}) and direction
Location of parcel at 900 m which left Cardington at time indicated (2100 in example) ● 21

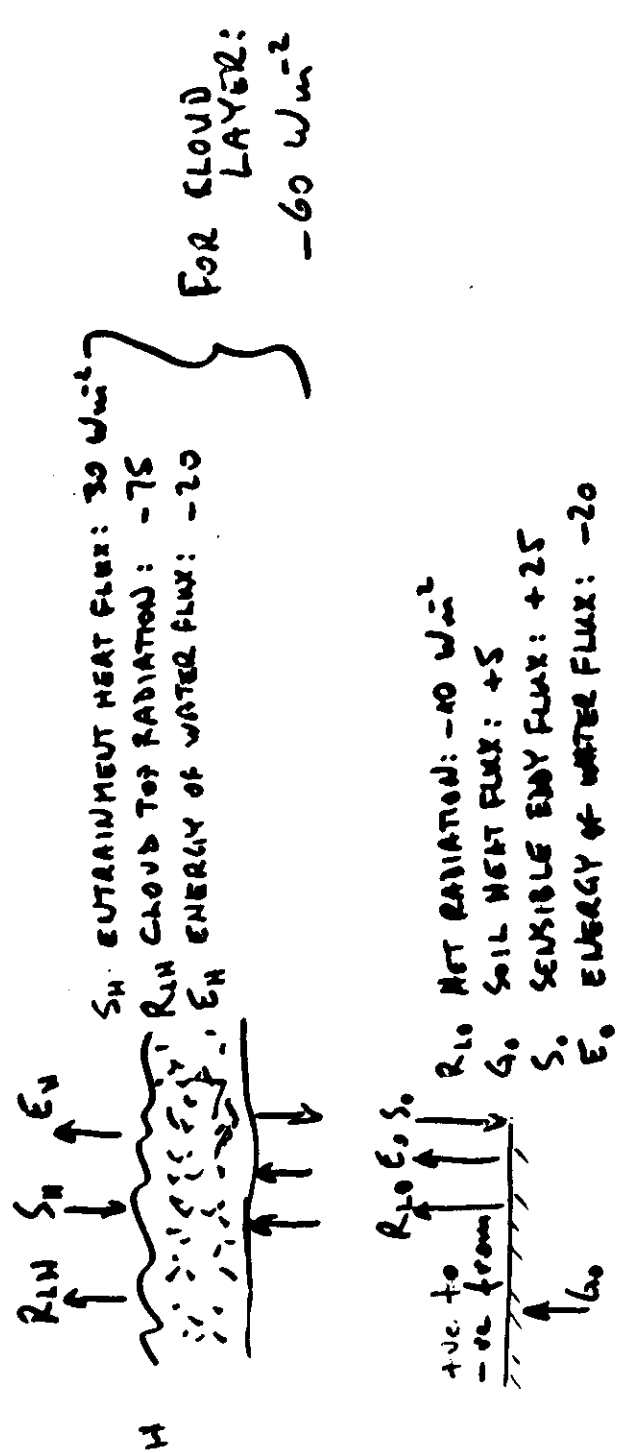

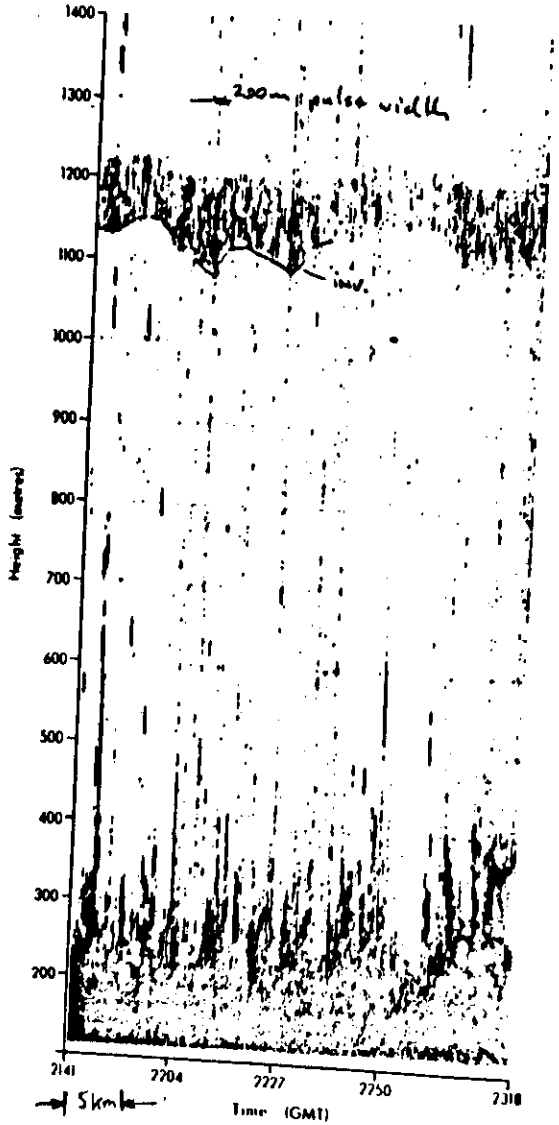

Figure 1. Acoustic sounder record for the period 2141–2318GMT on the night of 19 November 1976 at the MRU Cardington. Dark areas represent regions of strong echo.

at the top of the daytime convective boundary layer (Readings *et al.* 1973; Kaimal *et al.* 1976; Caughey and Palmer 1979) where intense convective plumes cause large distortions of the interface on a scale of several hundreds of metres, are readily detected by an acoustic sounder and result in local breakdown of the interface and possibly some overturning (Carson and Smith 1974) – the entrained air is drawn deep into the convective boundary layer by the return flows between thermal plumes and affect turbulence properties throughout the upper half of the boundary layer.

For nocturnal stratocumulus, it appears from Figs. 3, 4 and 6 that the turbulence is driven by buoyancy fluctuations near the top of the cloud layer. Blobs of relatively cold air may break away from the base of the EIL possibly dragging down filaments of warmer air. Deformation fields associated with these developing circulations may induce Kelvin-Helmholtz instabilities in the EIL which further assist entrainment. In the upper (radiatively

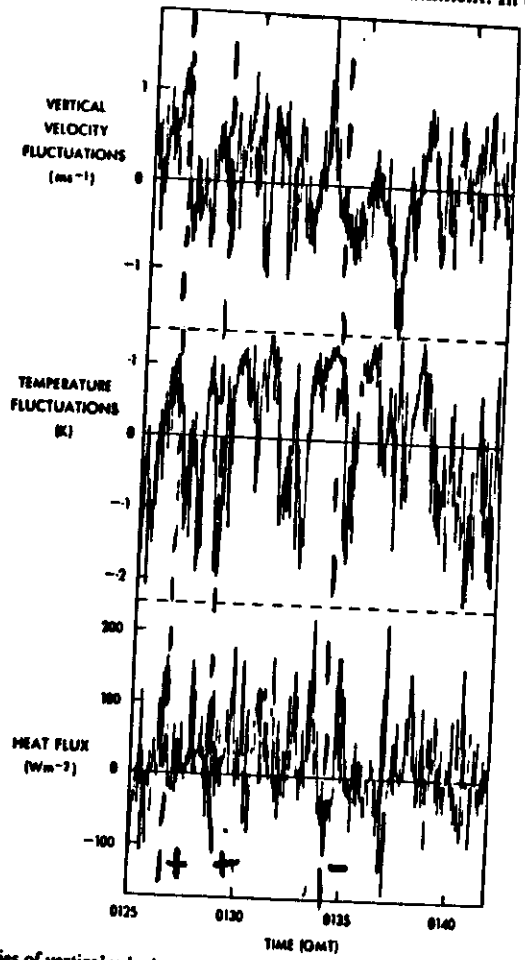

Figure 6. Time histories of vertical velocity, temperature and heat flux taken near the top of the cloud layer (z'/d around 0·95).

J. RECH. ATM. 1978

also have inhibited deeper convection (Fig. 3). Very small puffs of cumulus condensation were occasionally seen with bases at about 0.8 km height.

IV. — DYNAMICAL STRUCTURE IN CLOUD.

Although turbulent transfer is assumed to occur in stratiform cloud to partially balance the effects of radiant heating and cooling (see e.g. Paltridge, 1974a), there are no previous observations which indicate the nature of this turbulent motion. Records taken in cloud during this expedition suggest the possibility of some convective organization which exhibits a correlation between vertical motion and temperature fluctuations.

We therefore analyse the temperature and vertical velocity signals by a conditional sampling procedure which estimates separately the properties of fluid generally warmer than its surroundings and the properties of fluid generally cooler (Coulman, 1978b). In Figure 4 the normalized, conditionally expected vertical velocity w'', defined as

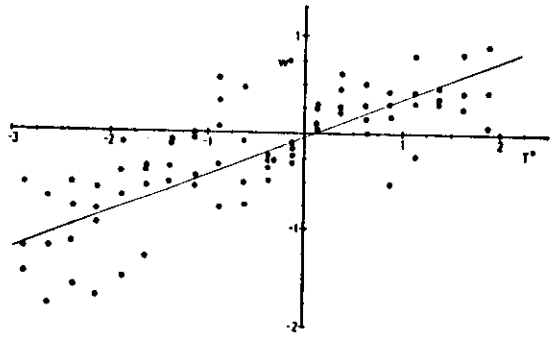

FIG. 4. — Data from four runs in cloud on 17 February show a linear trend of normalized vertical velocity fluctuation w'' with temperature fluctuation T'' for both positive and negative values of these variables.

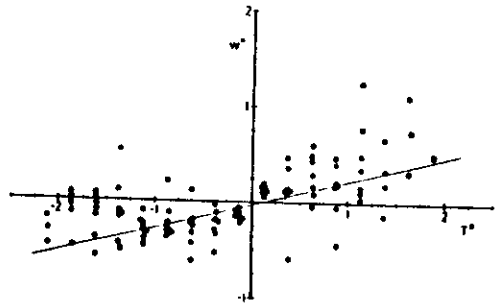

FIG. 5. — As for Figure 4 but the data are from three runs in cloud on 14 February and four on 15 February.

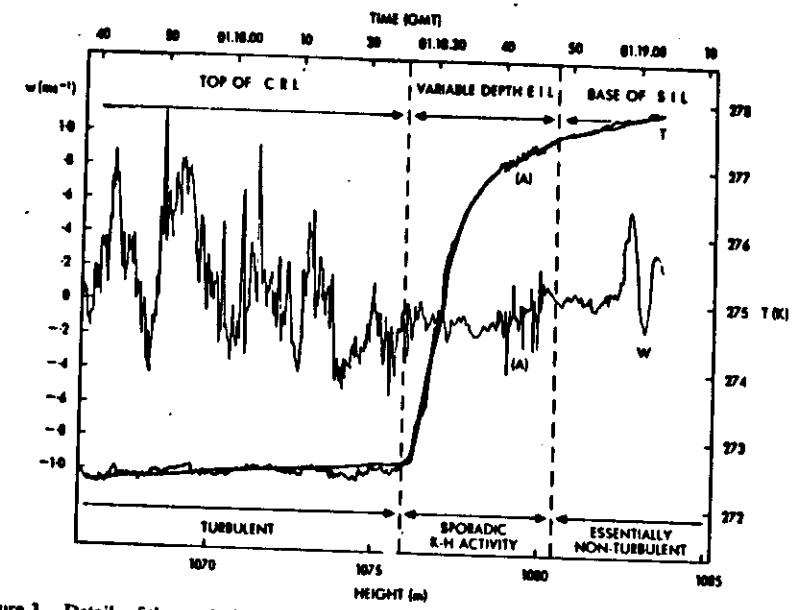

Figure 3. Details of the vertical velocity and temperature measurements taken during a traverse of the EIL when this was relatively non-turbulent. The feature 'A' is thought due to Kelvin-Helmholtz breakdown in a region where the Richardson number may have been reduced to around ¼ by wind shear. CRL denotes the cloud radiative layer; SIL the subsidence inversion layer.

4. Structure of the Entrainment Interfacial Layer

Examples of the detailed structure of the EIL observed on two transits are shown in Figs. 3 and 4, and Table I gives a summary of the main characteristics of 10 transits.

The location of the boundaries of the EIL were not always clear cut. In Table I the depth of the layer, Δh, containing most (4K) of the temperature jump has been taken as one measure of its thickness. This procedure was chosen because the shape of the temperature jumps are sometimes approximately exponential in shape without a clearly defined upper boundary, in contrast to the sharp lower boundary – the inversion base. Errors in estimates of Δh due to changing inversion base height (Fig. 2) during the period of traverse (10–30 s) are estimated to be less than 20%. The height difference between inversion base and cloud top ($h_i - h_c$ in Table I) suggests that these were coincident within the error of measurement.

The upper boundary of the EIL may also be defined by the extent to which turbulent vertical velocity fluctuations extend above the sharply defined inversion base. This is illustrated in Figs. 3 and 4 by two transits (3 and 8 respectively in Table I) of contrasting character. The upper boundary of the EIL thus defined usually lies above the upper level of

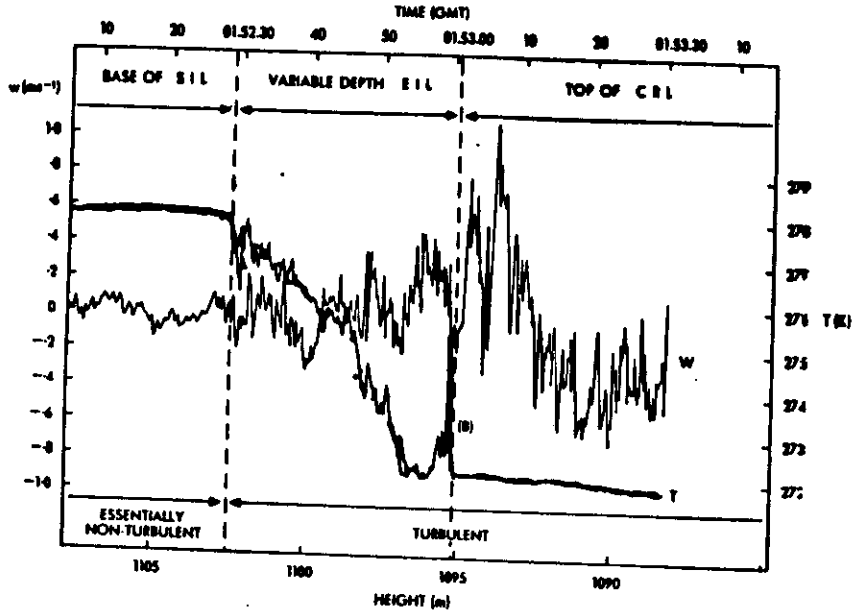

Figure 4. As Figure 3 for an occasion when the EIL was much deeper and fully turbulent. The feature 'B' is considered to be a volume of air in the process of entrainment.

in the very stable surface layer (Caughey and Readings 1975) and above the daytime convective boundary layer (Palmer *et al.* 1979). Figure 3 shows an EIL which may be in an early stage of breakdown into turbulence. A contrasting situation is illustrated in Fig. 4, where the layer is much deeper and turbulent velocity and temperature fluctuations fill the EIL. It may illustrate an occasion of complete turbulent breakdown of the layer. Woods (1969) has shown that the thickness of a thermally stable layer increases about four-fold as a result of turbulent breakdown, as is observed here. The clearer definition of the upper limit of the EIL in Fig. 4 may be due to turbulent erosion in this region. That the situation corresponds to active entrainment is supported by the feature labelled 'B' which appears to be a filament of warm air detaching from the EIL and mixing into the upper part of the cloud layer. Similar features were observed at the base of the EIL in other transits and provide the only direct evidence available for the scale of the entrainment process. As the local wind speed was much greater than the speed of ascent/descent of the balloon the scale of the entrained parcels appears to be about 10 m. Such small scale features would soon be mixed by the turbulence in the cloud top.

The possibility that breakdown of the thermally stable EIL results from the development of Kelvin-Helmholtz instability has to be considered. Figure 5 shows the profiles of wind speeds averaged over 30 s (about 10 m) corresponding to transits 4 and 6 which were respectively the occasions when the layer was thickest and thinnest. Clearly a considerably

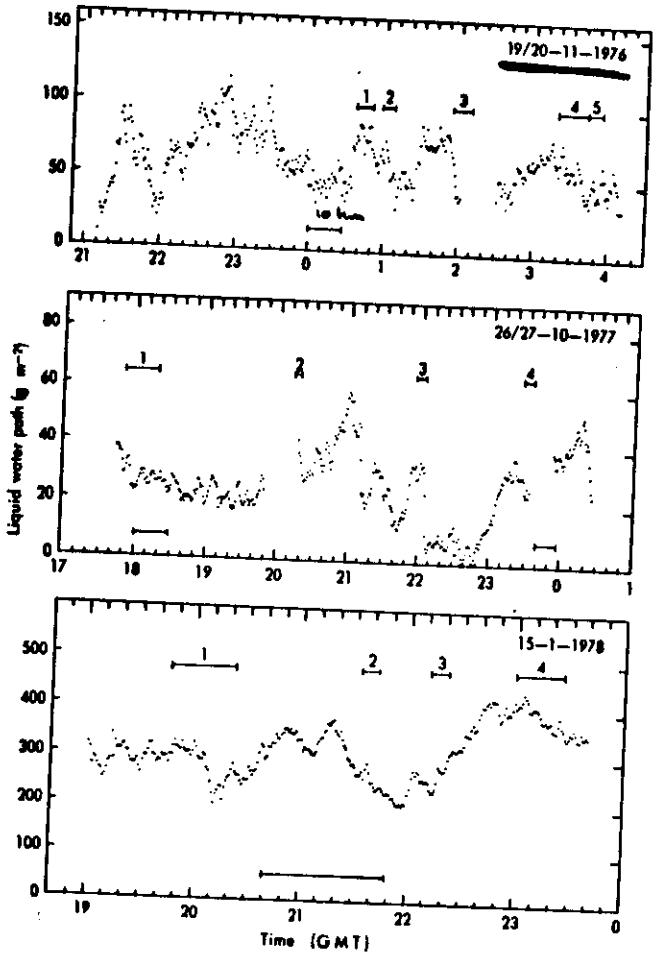

Figure 1. Time series of the integrated liquid water paths derived from the microwave radiometer data for the three case studies. The points are one minute averages. The numbered lines above the points indicate the times of the balloon profiles through cloud. The lines below the points indicate an advection distance of 10 km., calculated using the mean observed wind in the cloud layer at that time.

sonde and radiometer data. All three traces show high frequency variability due to irregularities on a spatial scale of about 1 km, superimposed on longer period drifts which pre-

gave the values which were used to scale the ASSP data.

The balloon observations for each of the three case studies will now be presented and discussed in section 5.

(a) 19–20 *November* 1976

This case study is discussed in detail in Paper I, where the profiles of temperature and humidity mixing ratio are presented. Table 2 compares the liquid water paths measured by the microwave radiometer with the values obtained by vertical integration of the ASSP liquid water content profiles and the theoretical values derived by assuming adiabatic ascent from cloud base to top. The liquid water path from the microwave radiometer is on average about 0·7 times the value for adiabatic ascent. The two ASSP liquid water content estimates are systematically larger than the microwave radiometer values and differ from each other by a factor of about 2. This indicates that the true sampling volumes are larger than the provisional values calculated theoretically by Roach (1977) and underlines the importance of an independent liquid water content estimate to calibrate ASSP data. To aid comparisons between the case studies, the provisional sampling volumes have been used throughout this table to calculate liquid water contents from the ASSP data.

Figure 2 illustrates the cloud microphysical data obtained with the ASSP during profile 1. The liquid water contents are the inner volume estimates, scaled by a single factor so that

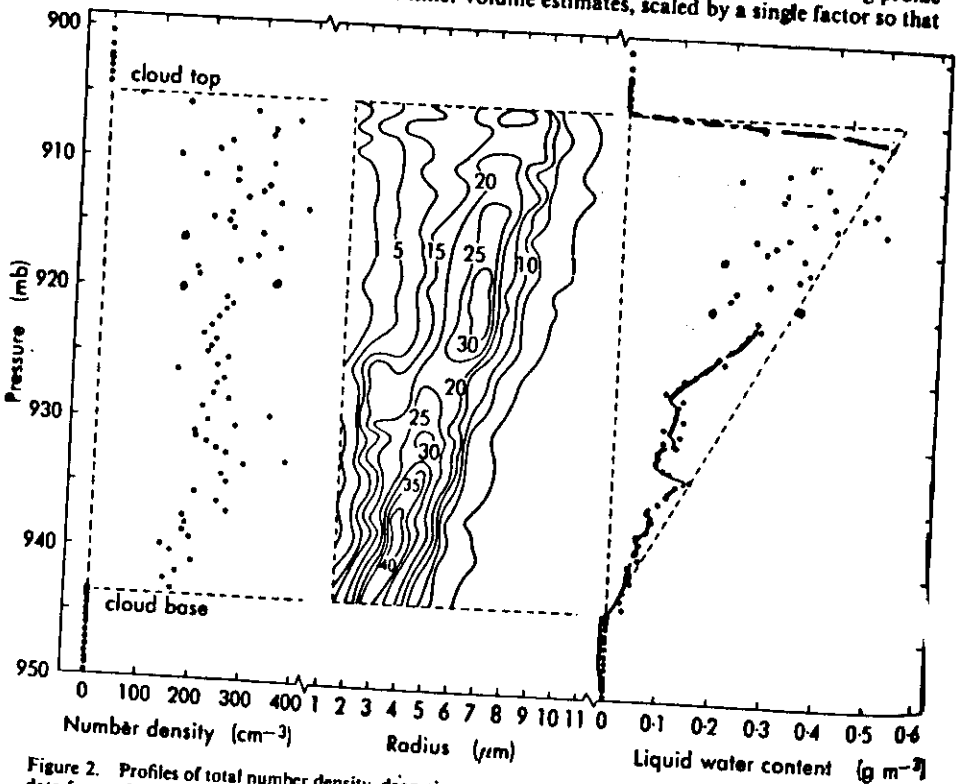

Figure 2. Profiles of total number density, drop-size spectra and liquid water content from the scaled ASSP data for profile 1, 19–20 November 1976. The drop-size spectra are presented as contours of the percentage normalized spectral density, such that at any height the sum of the values in each 1 μm interval is 100%. The liquid water content profile produced by adiabatic ascent from cloud base is shown as the dashed line.

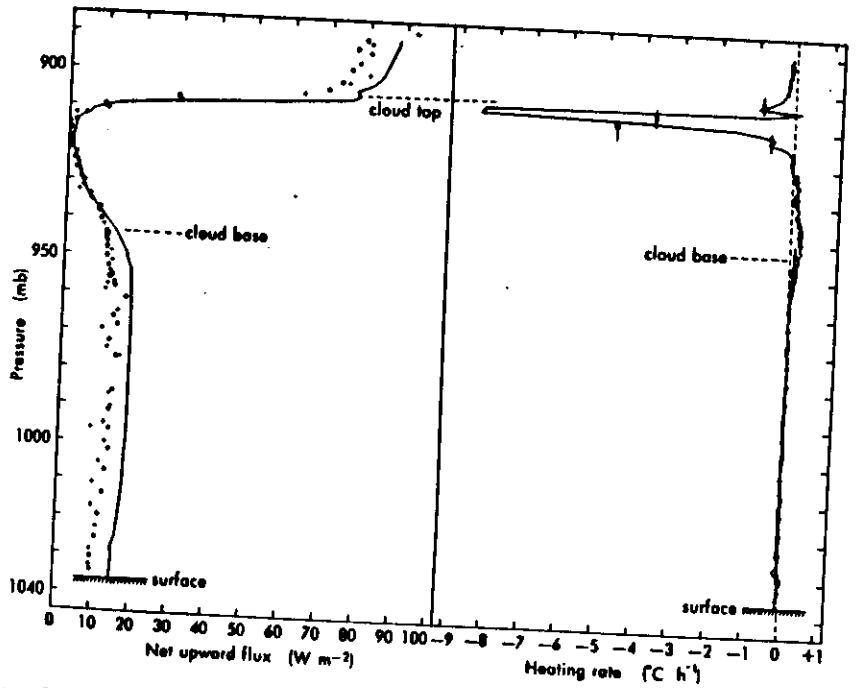

Figure 3. Comparison of the observed and theoretical net infrared fluxes and heating rates for profile 1, 19–20 November 1976. The continuous lines are from the radiation scheme, using the balloon temperatures and humidities and the scaled ASSP data. The dots and crosses represent the corrected fluxes from the upper and lower radiometers, respectively. Only every fifth value has been plotted.

High resolution net flux profiles through the cloud top are presented in Fig. 4. Only the first three profiles were used as the later profiles suffered from increased noise. The purpose of profile 2 was to investigate the cloud top entrainment structure so data well into the inversion were not obtained. The microwave radiometer was switched off during the latter part of profile 3, but this should not lead to appreciable error in the flux comparisons as data were obtained for the beginning of the profile when the balloon was traversing the cloud top. The solid curves indicate the theoretical profiles using the liquid water content estimates from the ASSP inner and outer volumes and also from the ASSP inner volume estimate, scaled by the microwave radiometer. The theoretical profiles for integrated liquid water paths of half and twice the microwave radiometer value are also shown. There is an uncertainty of about 0·5 mb in the positioning of the theoretical profiles owing to the 10 s sampling period and the resolution of the radiation scheme. The closeness of the theoretical curves makes it difficult to assess which is the best liquid water content estimate, but the outer

compared with aircraft observations (Stephens *et al.* 1978). The computational techniques used by Stephens and by Roach and Slingo (1979) are very different and it is interesting to compare the predictions of the two schemes. Stephens *et al.* (1978) noted poor agreement between the observed and predicted values of the effective downward emissivity, due to the large experimental errors. The effective downward emissivity may be defined as;

$$\varepsilon(p) = \{F(p)\downarrow - F(p_0)\downarrow\}/\{B(p) - F(p_0)\downarrow\} \quad . \quad . \quad (3)$$

The emissivity is calculated at pressure level p within the cloud, where the downward longwave flux is $F(p)\downarrow$ and the Planck function flux is $B(p)$. The downward flux at the cloud top is $F(p_0)\downarrow$. The radiometer observations presented here are of net flux only, so they cannot be used to calculate the emissivity directly. The values plotted on Fig. 13 were therefore

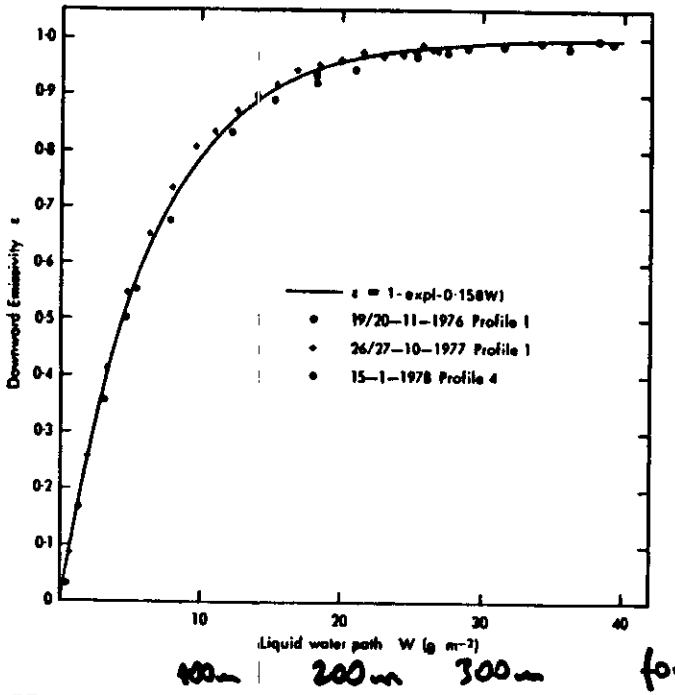

Figure 13. Effective downward emissivity as a function of liquid water path through cloud top, calculated by the radiation scheme for the three profiles indicated. Stephens (1978b) parametrized form of the emissivity is also shown.

calculated from the radiation scheme, using data from the three case studies. The solid curve represents the parametrized form of the effective downward emissivity which Stephens (1978b) fitted to the results from his theoretical model. This curve gives an excellent fit to the emissivities calculated here, indicating that, despite their different structure, the two schemes are essentially identical in their treatment of cloud liquid water. The goodness of fit and the small scatter about the parametrized curve also illustrate the well known insensitivity of the flux profiles to the drop-size distribution function and the minor role played by scattering (e.g. Paltridge and Platt 1976).

The shape of the net flux profiles and their position relative to the cloud top and